Autosub Long Range Derived Near Seabed Flow in the Western Flank of the Orkney Passage

Katie Rebecca Hodge
MSci Oceanography

Supervisor:
Dr Eleanor Frajka-Williams

3rd Year Project

2018

UNIVERSITY OF Southampton

Abstract

The Orkney Passage is a submarine valley in the South Scotia Ridge that connects the Scotia Sea to the Weddell Sea. It is the most direct throughflow for deep water outflow from the Weddell Sea to enter the Atlantic Overturning Circulation. This study uses autonomous underwater vehicle data from the Dynamics of the Orkney Passage Outflow Project (DynOPO) to investigate the near seabed flow in the western flank of the Orkney Passage and test the hypothesis that across slope flow in the region will primarily be downslope as a result of Ekman Veering. From assessing 28 locations across slope flow was observed to be predominantly in a downslope direction, occurring twice as often as upslope flow. It was found that 16 locations directly violate Ekman Veering, five locations somewhat conform to Ekman veering and the remaining locations neither support nor violate Ekman Veering. This lead to the conclusion that Ekman veering is not the only process responsible for the observed across slope flow in the region. Subsequently, other processes are briefly investigated. The Ekman layer thickness and the net across slope flow within the bottom boundary layer were also calculated.

Table of Contents

Acknowledgements

Thank you for the support and guidance from my supervisor Dr Eleanor Frajka-Williams and post doctorate researcher Dr Carl Spingys. Also thanks to Dr Alexander Forryan for helping me with the initial stages of Matlab and signposting me to appropriate bathymetry datasets. A composite of swath bathymetry data it used, produced by Povl Abrahamsen at the British Antarctic Survey. ADCP and CTD data are from the Dynamics of the Orkney Passage Outflow Project (DynOPO), a NERC funded project. Data analysis was carried out in Mathworks MATLAB.

1 Introduction

1.1 About the Orkney Passage

The Orkney Passage (OP) is a submarine valley in the South Scotia Ridge that connects the Scotia Sea to the Weddell Sea - a deep water forming region (Gordon *et al.*, 2001; Meredith *et al.*, 2000). It is the most direct throughflow (see Figure 1) where deep water outflow, Weddell Sea Deep Water (WSDW), enters the Atlantic Overturning Circulation (Naveira Garabato *et al.* 2002). WSDW is characterised by a potential temperature between 0 and -0.7°C and is the main contributor to Antarctic Bottom Water (AABW) (Meredith *et al.*, 2011). The Orkney Passage extends to depths in excess of 4000m and is characterised by a sill rising to 3600m that has been the subject of recent research (Naveira Garabato *et al.*, 2017; Polzin *et al.*, 2014; Meredith *et al.* 2011; Naveira Garabato *el al.* 2002). This study will focus on the western flank of the OP downstream of the sill. The western flank is steeply sloping from 1500m to 400m in just 10km (Figure 2).

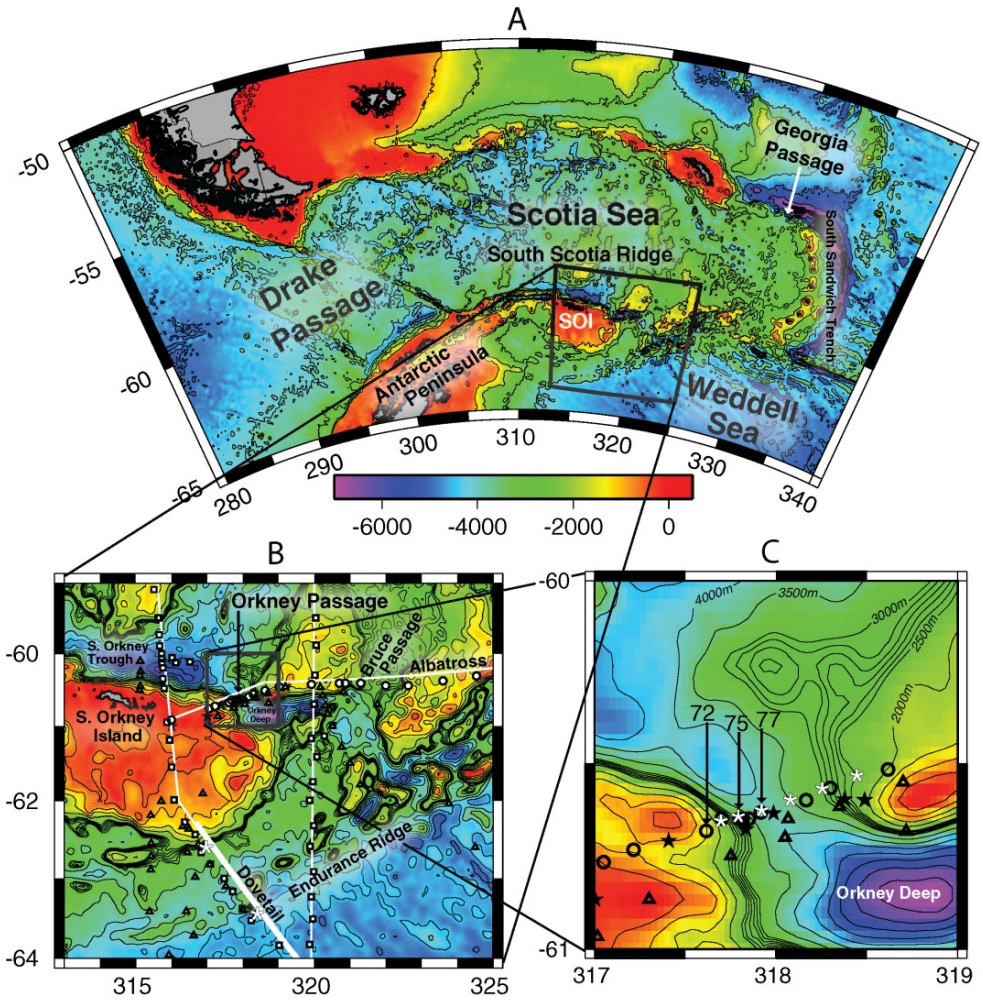

Figure 1: Overview of where the Orkney Passage is situated from Polzin et al. (2014). The circles, squares, triangles and stars in the bottom two panels denote existing datasets as outlined in Polzin et al. (2014).

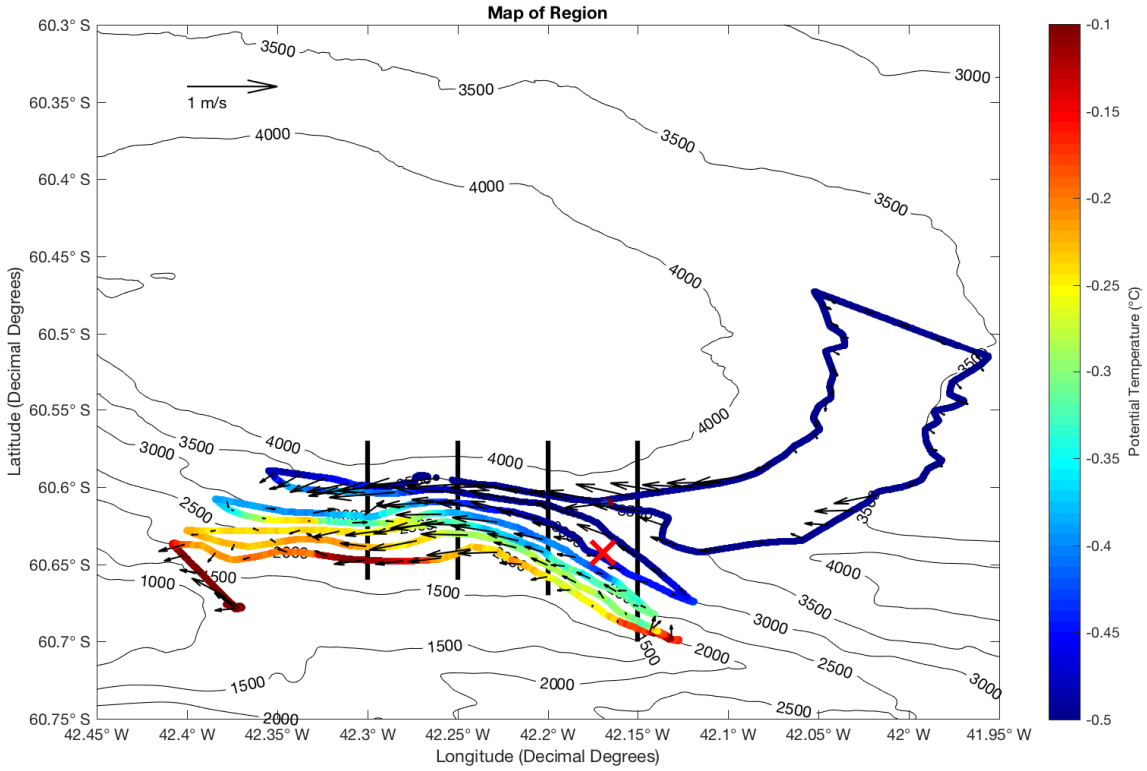

Figure 2: Overview Map of Western Flank of Orkney Passage. The black arrows are the rotated mean velocities of the bottom 200m of the water column. The potential temperature is recorded at the ALR height. The thick black lines are the across slope transects and the red 'X' is the location of the nearest CTD cast (62) from RRS James Clark Ross. Potential temperature and rotated velocities are averaged over 31 minute intervals.

Warming and contraction in volume of AABW in recent years (Purkey and Johnson, 2010) has motivated monitoring of WSDW in the Orkney Passage as it acts as a natural choke point. Previous surveys in the region include: The Deep Ocean Ventilation through Antarctic Intermediate Layers (DOVETAIL) (Gordon *et al.*, 2001); the Antarctic Large-Scale Box Analysis and the Role of the Scotia Sea (ALBATROSS) (Naveira Garabato *et al.*, 2002); and the Antarctic Deep Water Rates of Export (ANDREX) (Jullion *et al.*, 2014). This research has primarily focussed on the controls on WDWS with particular focus on wind forcing, turbulent mixing and bottom Ekman layer dynamics (Naveira Garabato *et al.*, 2017; Polzin *et al.*, 2014; Meredith *et al.*, 2011). Previous observations in the region were obtained from ship based Conductivity, Temperature, Depth (CTD) casts and lowered Acoustic Doppler Current Profilers (LADCPs). This study uses Autonomous Underwater Vehicle (AUV) data from Naveira Garabato *et al.* (2017), the first dataset of its kind, to focus on the dynamics of near seabed flow in the western flank of the Orkney Passage with the primary aim of identifying if there is upslope or downslope in the region.

1.2 Theory

Ekman (1905), hereafter referred to as Ekman theory, found that at the sea surface, the current direction is rotated 45° to the left (in the Southern Hemisphere) of the overlying wind stress. The current continues to rotate throughout an Ekman layer to a depth of z=-D_E where the ocean current is in the opposite direction to the wind. This results in the net direction of transport across the Ekman layer being 90° to the wind direction. $\mathrm{D_E}$, the Ekman depth, is defined as the vertical influence the stress has on the water column (Simpson and Sharples, 2010).

Ekman theory can also be applied to near seabed flow, where seabed friction acts as the stress and results in a bottom layer structure similar to that at the surface. Interior flow (u_g) well away from the seabed is in geostrophic balance with only the pressure gradient force and the Coriolis force involved. This assumes the flow is linear, steady, and inviscid (frictionless).

$$f u_g = -\frac{1}{\rho_0}\frac{\partial p}{\partial y} \tag{1}$$

Over steeply sloping topography such as the Orkney Passage the geostrophic interior flow is topographically steered at all levels according to the Taylor – Proudman theorem. As summarised by Simpson and Sharples (2010), the Taylor-Proudman breaks down under one of three scenarios: 1) if the flow is unsteady, 2) the flow is so vigorous that the non-linear terms become important, 3) frictional effects are important.

Near the seabed, flow is influenced by friction, resulting in ageostrophic flow perpendicular to the overlying interior flow direction. For a flat seabed the equations of motion are:

$$0 = fv - \frac{1}{\rho_0}\frac{\partial \tau_x}{\partial z} \qquad \text{and} \qquad 0 = -fu - \frac{1}{\rho_0}\frac{\partial \tau_y}{\partial z} + f u_g \tag{2}$$

The seabed stress can then be expressed in terms of vertical shear and eddy viscosity. Resulting in a balance between the Coriolis force and a vertical stress divergence in the Ekman layer (Polzin *et al.*, 2014).

$$-fv = N_z \frac{\partial^2 u}{\partial z^2} \qquad \text{and} \qquad f(u - u_g) = N_z \frac{\partial^2 v}{\partial z^2} \tag{3}$$

However, on a sloping boundary such as the western flank of the OP that has a ¼ to 1/5 gradient (Polzin *et al.*, 2014) the Ekman layer is governed by a balance between the Coriolis force and the pressure gradient force (Trowbridge and Lentz, 1991; MacCready and Rhines, 1993; Brink and Lentz, 2010). Friction slows the current near the seabed so that the Coriolis force is reduced. This leads to an unbalanced pressure component which drives across slope flow (either upslope or downslope) known as

Ekman Veering. Across slope flow results in horizontal gradients characterised by isopycnals bending towards the seabed (Brink and Lentz, 2010; Polzin et al., 2014). Regardless of the direction of Ekman veering, the horizontal density gradient brings the along slope velocity to rest at the seabed, giving the boundary conditions of $u = 0, v = 0$ at $z = 0$ (Brink and Lentz, 2010). The vertical extent of the influence the seabed has on the interior flow is known as the bottom boundary layer (BBL), this region is characterised by turbulent flow and extends from the seabed to a height of 99% of the free stream velocity (the interior velocity).

The slowing of the along slope flow near the seabed results in an Ekman spiral. In the Southern Hemisphere, flow is rotated to the right (clockwise as you approach the seabed) of the overlying along slope interior flow direction. Under a constant viscosity bottom boundary layer, it is predicted at the seabed that the current will have veered 45° clockwise of the overlying interior geostrophic flow direction. However observational studies show in reality this rotation rarely exceeds 20° (Perlin *et al.* 2007; Simpson and Sharples, 2010).

Despite only a few observational studies focussing on Ekman theory in the BBL (Perlin *et al.*, 2007), Polzin *et al.* (2014) found a downwelling Ekman layer on the western side of the Orkney Passage that experiences relatively large scale vertical overturning associated with tidal forcing. This study uses AUV data to further investigate the behaviour of flow in the BBL in the western flank of the OP. A fixed BBL of 50m (BBL_{50}) is used to test the hypothesis that across slope flow in the region will primarily be downslope as a result of Ekman Veering.

2 Data

With the exception of Bathymetry data, all details discussed in this section can be found in the Cruise Report JR16005 (Naveira Garabato *et al.*, 2017).

2.1 Data Sources

The data used to assess the near seabed flow in the western flank of the OP is obtained from Autosub Long Range (ALR), an AUV developed at the National Oceanography Centre Southampton and known to the public as *Boaty McBoatface*. ALR was deployed on RRS *James Clark Ross* Cruise JR16005, March – May 2017 as part of the Dynamics of the Orkney Passage Outflow (DynOPO) project. The project is a collaboration between the British Antarctic Survey (BAS), the University of Southampton and the National Oceanography Centre Southampton.

The ALR undertook several missions, this study will only focus on data from the M44 mission: 18/04/17 20:54 UTC - 22/04/17 02:00 UTC. ALR traversed tight

switchbacks on the western flank of OP, traversing along isobaths approximately every 250m change in water depth. Giving a total ALR track length of 178km. The ALR was equipped with an upwards and downwards looking Teledyne RDI 300kHz Workhorse Acoustic Doppler Current Profiler (ADCP) and a Sea-Bird Electronics 52-MP CTD system. This provides a spatial view of near seabed velocities and ocean properties (Naveira Garabato *et al.,* 2017).

Velocity data was recorded using upward and downward looking ADCPs. Data is available from 65m above and below the vehicle giving a total range of 130m. Temperature, conductivity and pressure were record using an on-board CTD, this was only measured at the depth the ALR was at. CTD casts were also taken from RRS *James Clark Ross*, the nearest CTD cast to the region is CTD cast 62 (see Figure 2) (Naveira Garabato *et al.,* 2017).

Swath bathymetry data was used for the Orkney Passage region from a composite of multiple research cruises on RRS *James Clark Ross* in the region, produced by Povl Abrahamsen at BAS.

2.2 Data Processing

The ADCP data this study uses is pre-processed as described in the cruise report JR16005 (Naveira Garabato *et al.* 2017). Key points to note are that the data is sound speed corrected using ALR CTD data (N.B. the ALR CTD data is unprocessed), bad data has been removed and the upward and downward looking ADCP data has been recombined and gridded onto a common time grid. The velocity used for this study is binned into 8m bins with increasing height above seabed to a maximum of 200m and has a time step of one minute.

The procedure for removing data involved the blanking of data in the bin nearest the vehicle in both the upwards and downwards looking data sets. Near bottom bad data (large amplitude and large variance) in the downwards looking ADCP was also removed. Bins 74-98m from the ALR were blanked. It is important to note that despite attempts to remove bad data, some spikes still remain in the velocity data and should be treated with caution. This will be imperative when analysing near bottom velocities, especially those within the BBL.

As mentioned previously, ALR CTD remains unprocessed. Although the CTD data is used in this study to provide information of the potential origin of water masses, no attempt is made to process the data. This decision is made as the temperature data is only compared relative to each other and the explicit values are not required. However, unlike the ALR CTD data, the ship-based CTD data (e.g. CTD cast 62) has been processed so can be referred to explicitly.

3 Methods

3.1 Extracting the Velocity Data

This report will primarily focus on four across slope transects at 42.15°W, 42.20°W, 42.25°W and 42.30°W (these four transects were chosen based on Figure 2). Data was extracted from a longitudinal range of ±0.003° and grouped into depth intervals corresponding to seven isobaths. The isobaths range from 2000-3500m in 250m increments, this gives a total of 28 locations. The depth range used to group data is shown in Table 1.

Table 1: Depth ranges used to group data at each transect to corresponding isobaths.

Group Number	Depth range (m)
1	>1800 - <2000
2	>2001 - <2310
3	>2311 - <2500
4	>2501 - <2710
5	>2711 - <3010
6	>3011 - <3300
7	>3301 - <3500

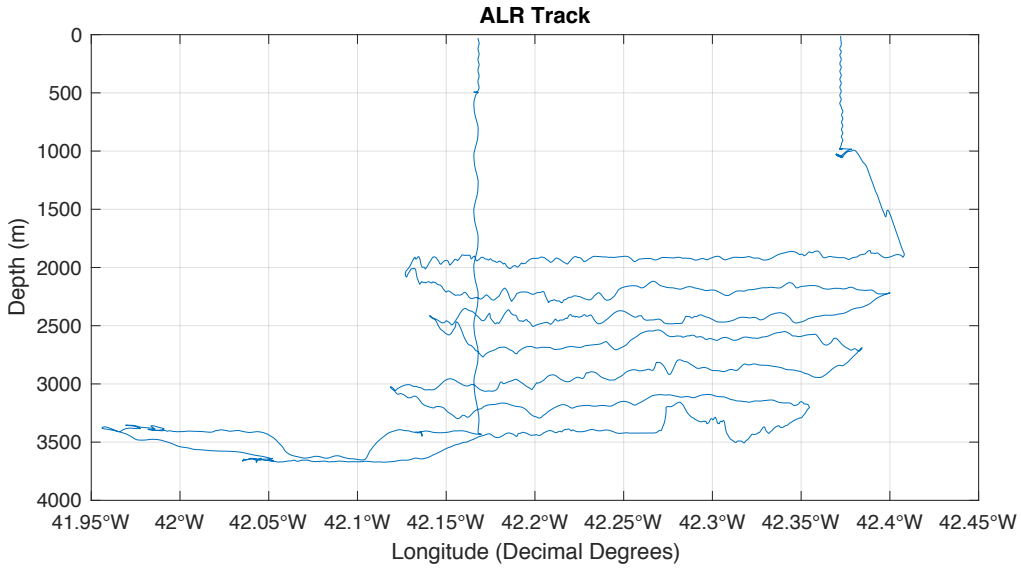

Figure 3: ALR Track. Note the locations are ship board estimates of the ALR. No attempt has been made to verify them.

As ALR didn't remain at a constant depth for each isobath (Figure 3), for each transect the grouping was checked to ensure the grouped data points lay on the correct segments of the ALR track that correspond to each isobath. At each transect each isobath had between 10 to 20 vertical profiles that were then averaged to form

a representative of the bottom 200m of the water column at each location. For transect 42.15°W the data points that lie on the ALR track after it has returned from traversing the sill (Figure 2) are removed as this is where the ALR begins its ascent back towards the surface.

3.2 Rotating Velocity Vectors

In order to determine if flow within the BBL was upslope or downslope, velocity vectors were rotated to give an along slope (u) and across slope (v) component. The vectors were rotated using the mean angle of the interior flow (all velocities >96m above the seabed). The depth threshold of >96m was chosen as this is well away from the seabed and the BBL. Once data is rotated, the sign convention remains so that eastward and northward flows are positive. This means that in the western flank of the OP, along slope flow (westward) is negative and downslope flow (northward) is positive.

3.3 Interior and Bottom Boundary Layer Flow

Based on a fixed BBL thickness of 50m (BBL_{50}) the vertical profile of each location is categorised as BBL flow and interior flow. Defined as 0-48m and 49-200m respectively. These ranges were chosen as the data is binned in 8m bins with increasing height above the seabed.

The BBL and interior flow are then used to asses the hypothesis for each isobath at each transect:

1) Across slope velocities in the BBL are assessed to identify if downslope (positive velocities) or upslope (negative velocities) flow is present.
2) The BBL across slope flow is then compared to the interior along slope flow to indicate if the across slope flow is likely to occur due to Ekman veering.
3) If flow appears to occur due to Ekman veering the magnitude of the BBL and interior flow are compared to further indicate if the flow occurs due to Ekman veering.
4) Finally, the flow direction of each layer in the water column was then analysed to help further decide if across slope flow was as a result of Ekman veering.

Additionally, to help characterise the flow at each transect the coefficient of determination (R^2) was calculated using a linear regression line to assess the strength of the correlation between the mean interior flow (dependent variable) and mean BBL flow (independent variable) calculated at each location.

3.4 Quantifying the Ekman Depth

3.4.1 Method 1: Unstratified Case

Method 1 originates from a numerical solution of the thickness of the planetary boundary layer (Hanna, 1969) and has commonly been applied to the ocean to calculate the thickness of bottom Ekman layer that is neutrally stratified (including the layers directly above it) (Perlin *et al.*, 2007).

$$D_{E1} = 0.2 \times \frac{u_*}{f} \quad (4)$$

Where f is the Coriolis parameter and u_* is the friction velocity (defined in Section 3.4.3).

3.4.2 Method 2: Stratified Case

Method 2 originates from Pollard *et al.* (1973) and is used when the bottom Ekman layer is unstratified but the layers directly above it are stratified. To account for the stratification, the buoyancy frequency N is included in the equation:

$$D_{E2} = \frac{K u_*}{\sqrt{Nf}} \quad (5)$$

Where K is a proportionality constant (1.7) (Perlin *et al.* 2007), u_* is the friction velocity, N is the stratification of the layer adjacent to the bottom mixed layer (representing ambient stratification) and f is the Coriolis parameter. Here, N is the square root of N^2, the Brunt-Vaisala frequency. As the ALR data only contains CTD data from the cruise height of the ALR, N^2 was calculated from CTD cast 62 using the CSIRO SeaWater EOS-80 toolbox. This uses the equation from Gill (1982):

$$N^2 = \frac{-g}{\rho_\theta} \frac{\partial \rho_\theta}{\partial z} \quad (6)$$

The deepest value of N (at 3121m) was then used in $DE2 = \frac{K u_*}{\sqrt{Nf}}$ (*5* to determine the Ekman depth. This is based on the assumption that N is a similar magnitude near the seabed at each transect.

3.4.3 Calculating the Friction Velocity

The friction velocity u_* is calculated using the following equation (Perlin *et al.*, 2007)

$$u_* = \sqrt{K_b U^2} \quad (7)$$

Where K_b is the bottom drag coefficient = 0.003 (non-dimensional) and U is the along slope velocity. Here U is defined as the mean along slope flow between 48-

64m above the seabed. 48m was chosen as a threshold as it is the nearest seabed height where there is both along and across slope velocities for the four transects.

3.5 Net Across Slope Transport

The net across slope transport was calculated at each transect for a fixed bottom boundary layer (BBL_{50}) by integrating the across slope velocities over the BBL thickness following Simpson and Sharples (2010).

$$\int_0^\infty v\, dz = \frac{u_g D_E}{2\pi} \quad (8)$$

Where u_g is the magnitude of mean along slope interior flow well away from the bottom boundary layer (as defined in Section 3.3).

4 Results

4.1 General Overview of the Region

Figure 2 is an overview map of the region showing preliminary results of potential temperatures and velocities. The potential temperature is from ALR height and is unprocessed whilst the velocity vectors are the mean rotated velocities of the water column. Figure 2 shows that potential temperature decreases downslope and along isobaths (moving East-West) with the coldest potential temperatures in the deepest part of the sill.

The interior flow is generally along slope (westward) and barotrophic (depth independent). Strongest velocities are between 42.25°W and 42.30°W at the 3000-3500m isobaths. West of 42.30°W between the 2000-3000m isobaths the flow is very weak with no consistent direction. Similarly, East of 42.17°W flow is very weak at the 2000-3000m isobaths with inconsistent flow direction at 2000 and 2250m isobaths including northward flow at 2000m isobath East of 42.15°W. Another area of interest is a warm patch at 2750m extending from approximately 42.335-42.355°W. Compared to the interior flow direction along the isobath further upstream, the flow direction is reversed (eastward). Linked to the interior flow above, the largest net across slope transport was observed at 42.25°W (3.2 m^2s^{-1}) and the smallest across slope flow as observed at 42.15°W (0.78 m^2s^{-1}). The mean net across slope flow for the four locations combined is 1.8 m^2s^{-1}).

4.2 Where is There Across Slope Flow in the BBL?

Figure 4-Figure 7 show the across slope transects from 42.15°W-42.30°W respectively, positive (negative) across slope velocities indicate downslope (upslope) flow. For all 28 locations there is across slope flow in the BBL_{50} , the only exceptions being 2750m isobath at 42.25°W where the across slope component was 0±0.013 m/s and the most downslope locations at 42.15°W and 42.25°W where no data was available in the BBL. As summarised in Figure 8 downslope flow occurs twice as often as upslope flow, additionally a combination of the two occurs at five other locations. The transect with the highest number of locations exhibiting downslope flow is 42.20°W. Generally, the magnitude of the across slope flow decreases with height above the seabed and increases in the BBL when the interior along slope flow increases. Further comparisons between the magnitude of the interior and BBL flow were then calculated to characterise the flow, as outlined in Section 4.3 below.

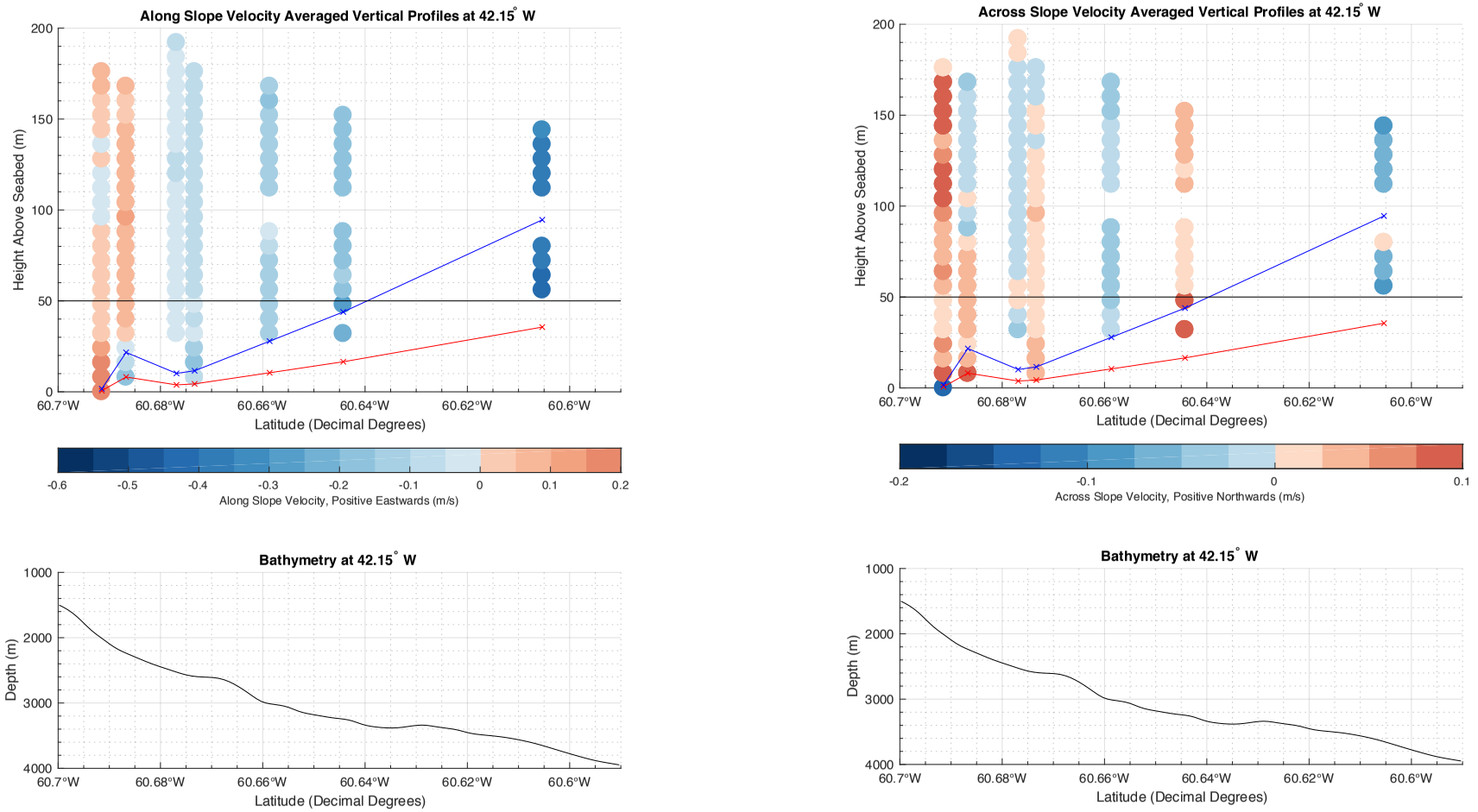

Figure 4: Top panels: Vertical Profiles of the along and across slope flow at 42.15°W. Positive velocities (eastward or downslope) are in red hues and negative velocities (westward or upslope) are in blue hues. The red and blue lines are the Ekman layer thicknesses calculated by method 1 and 2 respectively. Bottom panels: Bathymetry of the cross section.

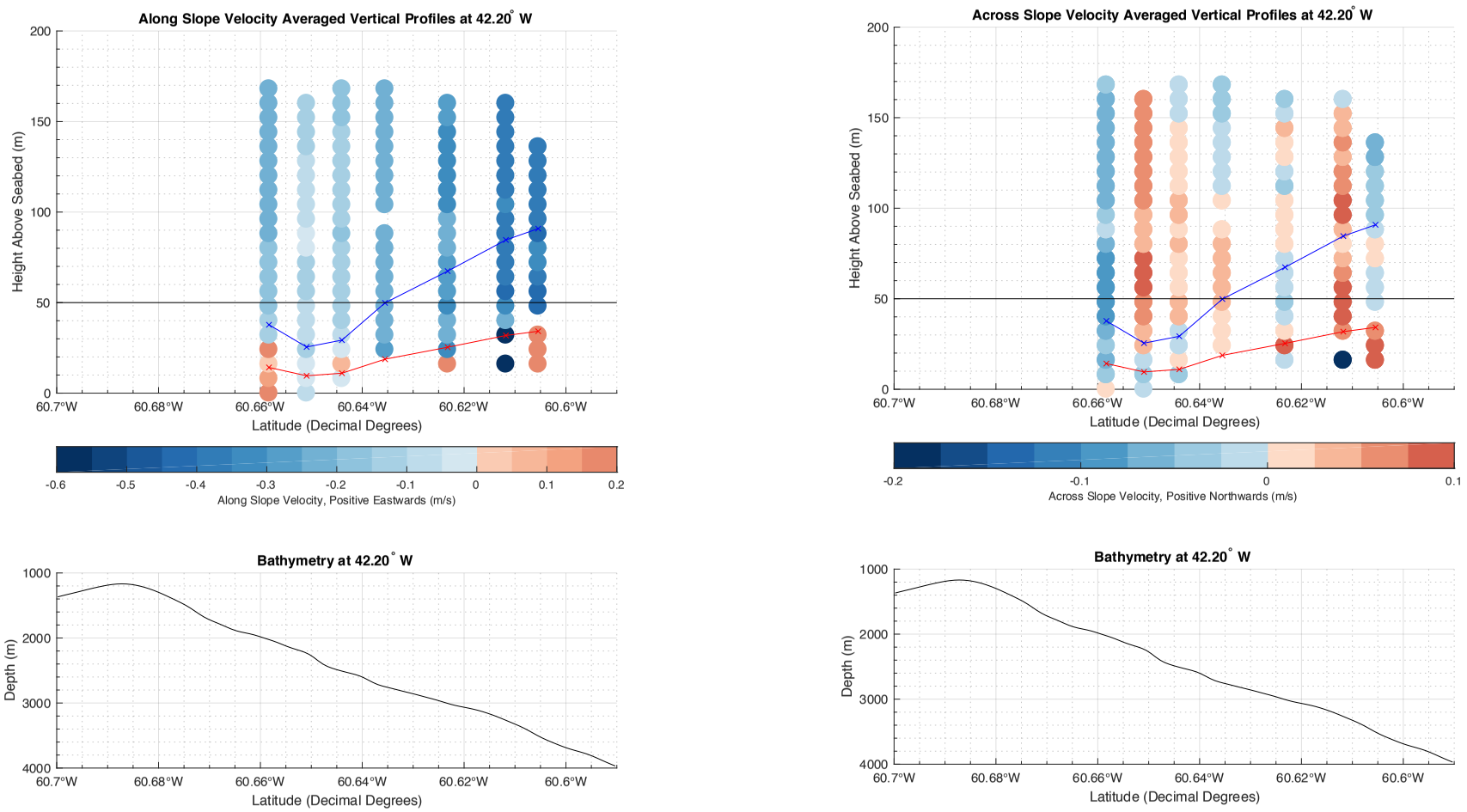

Figure 5: Top panels: Vertical Profiles of the along and across slope flow at 42.20°W. Positive velocities (eastward or downslope) are in red hues and negative velocities (westward or upslope) are in blue hues. The red and blue lines are the Ekman layer thicknesses calculated by method 1 and 2 respectively. Bottom panels: Bathymetry of the cross section.

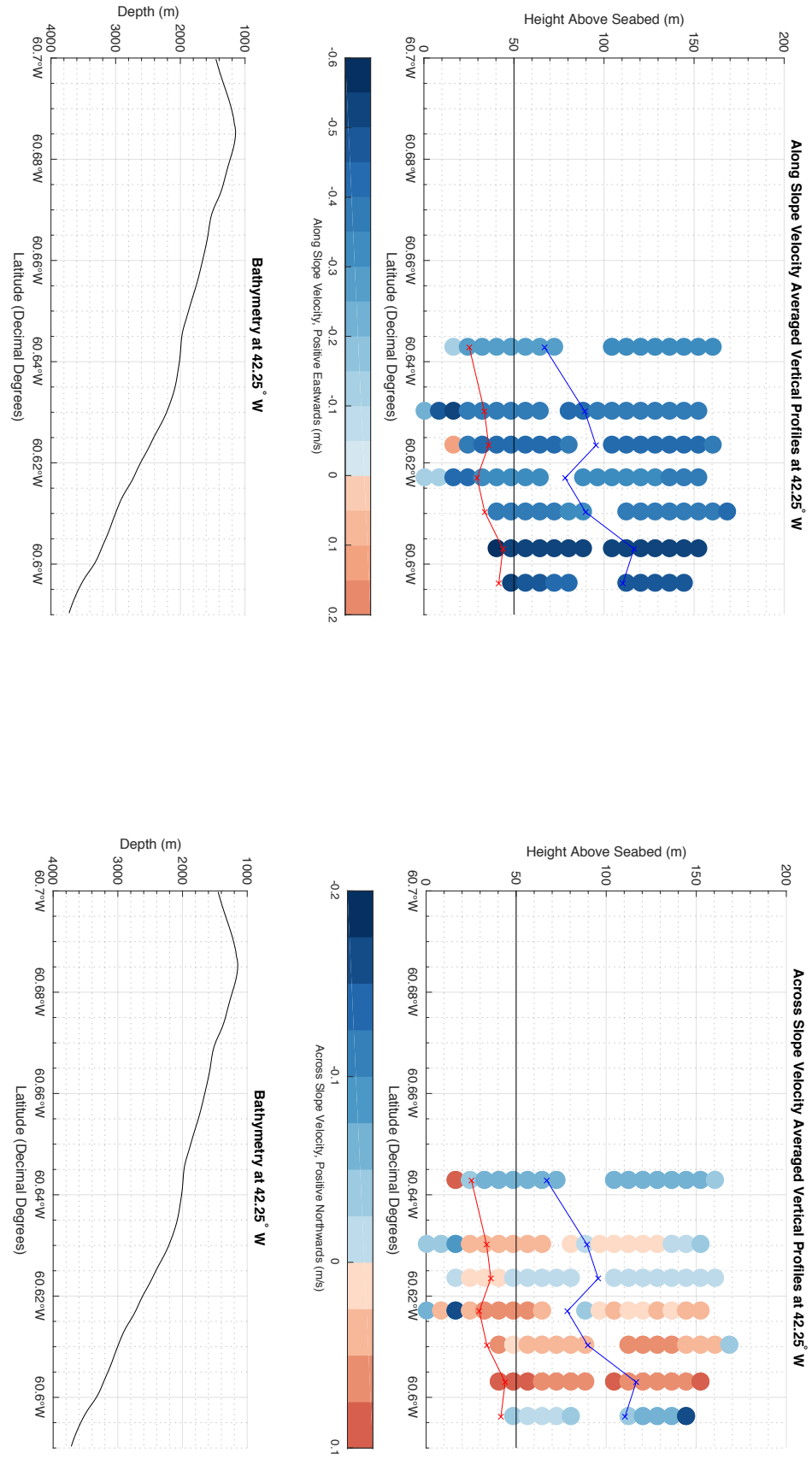

Figure 6: Top panels: Vertical Profiles of the along and across slope flow at 42.25°W. Positive velocities (eastward or downslope) are in red hues and negative velocities (westward or upslope) are in blue hues. The red and blue lines are the Ekman layer thicknesses calculated by method 1 and 2

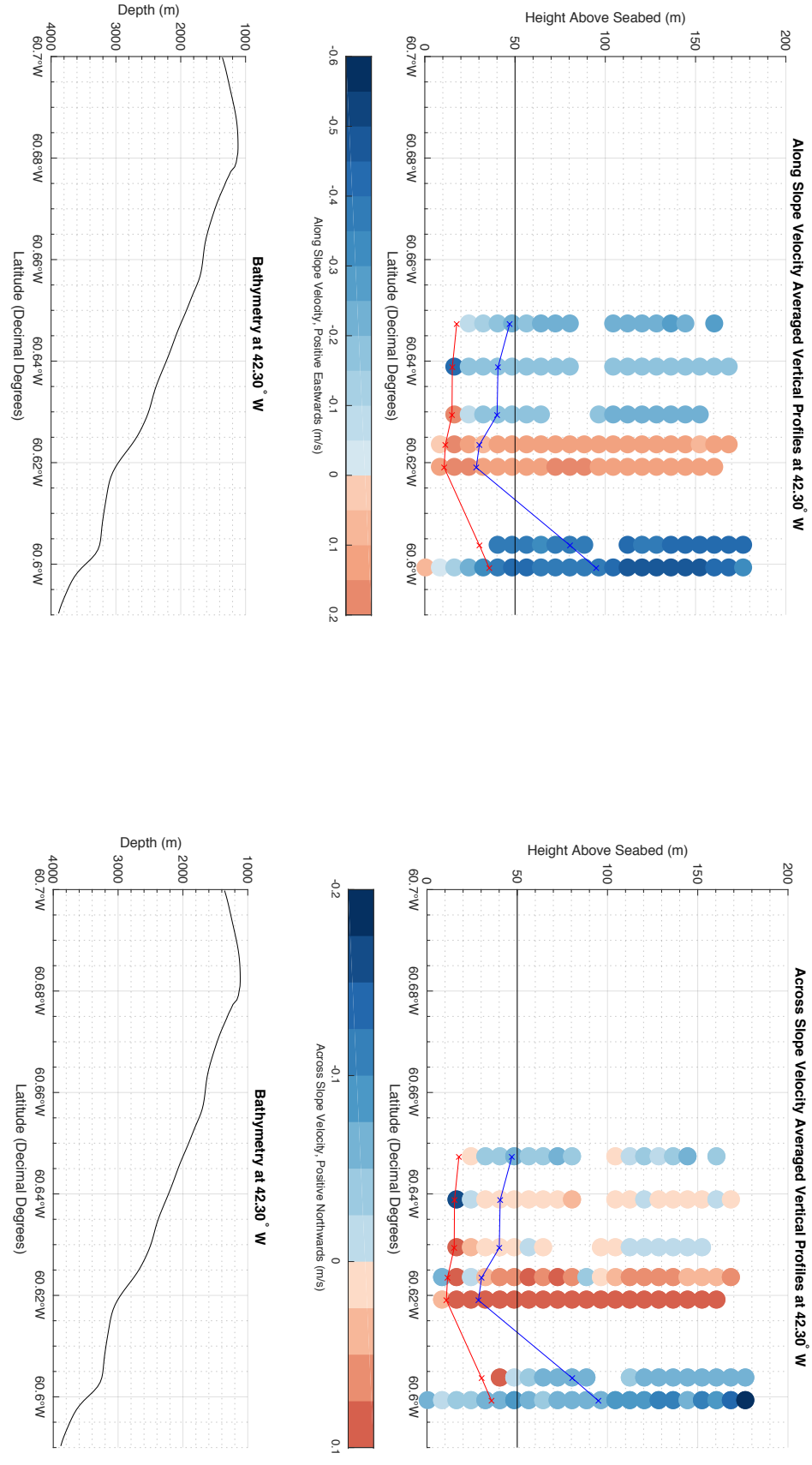

Figure 7: Top panels: Vertical Profiles of the along and across slope flow at 42.30°W. Positive velocities (eastward or downslope) are in red hues and negative velocities (westward or upslope) are in blue hues. The red and blue lines are the Ekman layer thicknesses calculated by method 1 and 2

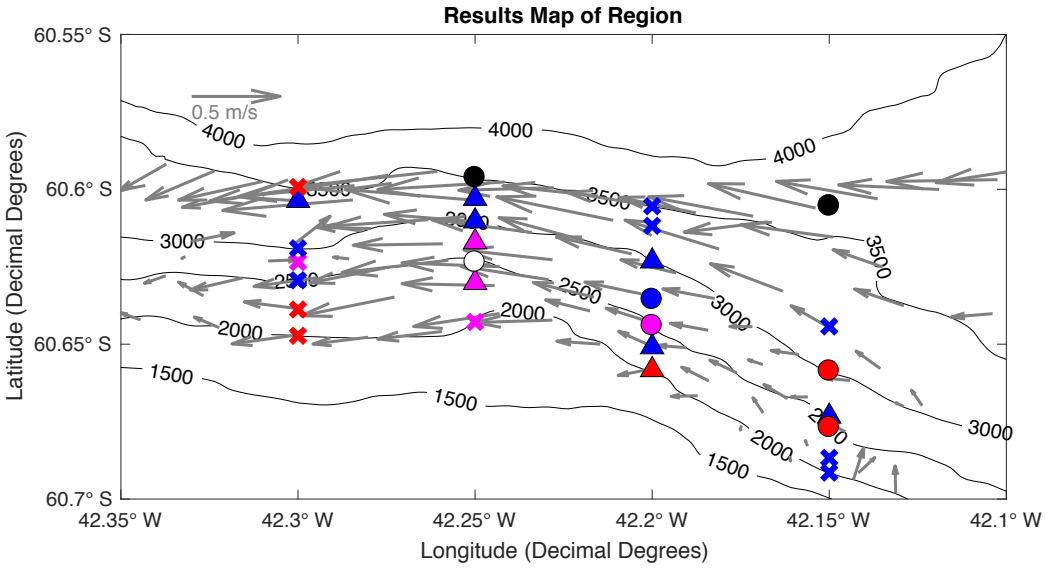

Figure 8: Results Map of the four transects. The colours of each symbol correspond to if the flow is: upslope (red), downslope (blue), neither (white), or a combination of the two (magenta). Where there is no data in the BBL the symbol is filled black. Neither is defined as when the across slope flow of the component is 0±0.013 m/s for the entire depth of the BBL. A combination of both upslope and downslope flow is defined when there is a layer of water flowing upslope/downslope overlying another layer of water flowing in the opposite direction (e.g. 0-20m is flowing downslope and 25-50m is flowing upslope). The different shaped symbols denote if the flow: conforms the Ekman theory (squares); partially conforms the Ekman theory (triangles); neither supports nor violates Ekman theory (circles); or violates Ekman theory.

4.3 Relationship Between Interior and BBL Flow

The coefficient of determination (R^2) was calculated between the mean interior flow (independent variable) and mean BBL flow (dependent variable) for a number of scenarios. For the four transects combined, a strong correlation $R^2 = 0.82$ to a 99% confidence level was found between mean interior along and mean BBL along slope flow. Interpreted as, 99% of the variance in the mean BBL along slope flow can be explained by the variance in the mean interior along slope flow. All locations fall well on the linear regression line (Figure 9), 42.15°W is characterised by the smaller magnitudes whilst 42.25°W is characterised by the larger magnitudes. This is consistent with Figure 2. A weak correlation $R^2 = 0.115$ to a 92% confidence level was calculated for the mean interior across slope and mean BBL across slope flow.

For the mean interior along and mean BBL across slope flow, for the four transects combined, $R^2 = 0.0158$ to a 47% confidence level. R^2 was also calculated for each transect individually as shown in Table 2. The strongest correlations occur at 42.15°W and the weakest occur at 42.25°W. It should be noted that for 42.30°W a weak negative correlation was observed as shown in Figure 10.

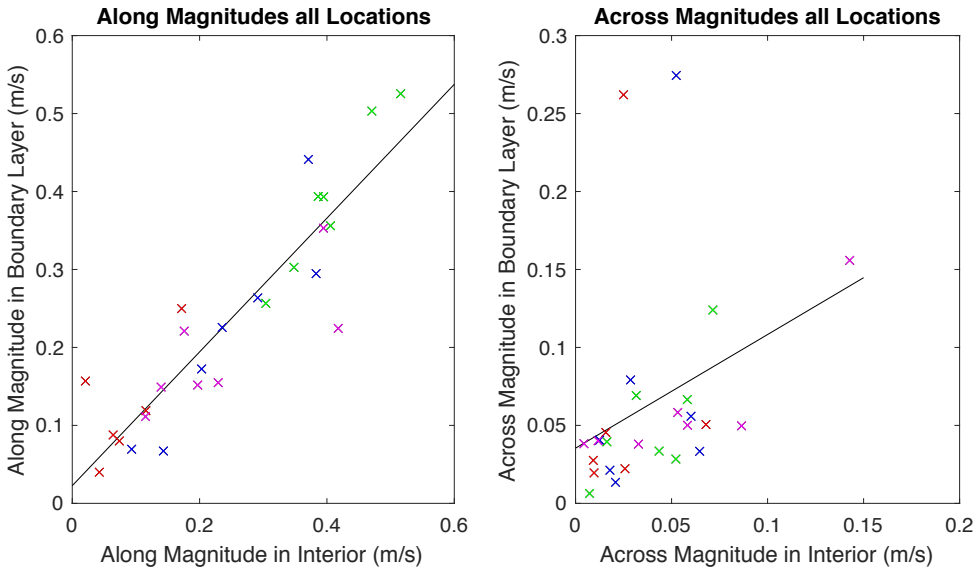

Figure 9: a) Comparison of along slope magnitudes b) across slope magnitudes for all four transects: 42.15°W (red), 42.20°W (blue), 42.25°W (green) and 42.30°W (magenta).

Table 2: Correlation between interior along slope flow and Ekman across slope flow for each transect.

Location (°W)	R^2 to 3sf	p-value to 3sf	Confidence Level (%)
42.15	0.590	0.075	93
42.20	0.386	0.136	87
42.25	0.073	0.557	44
42.30	0.114	0.460	54

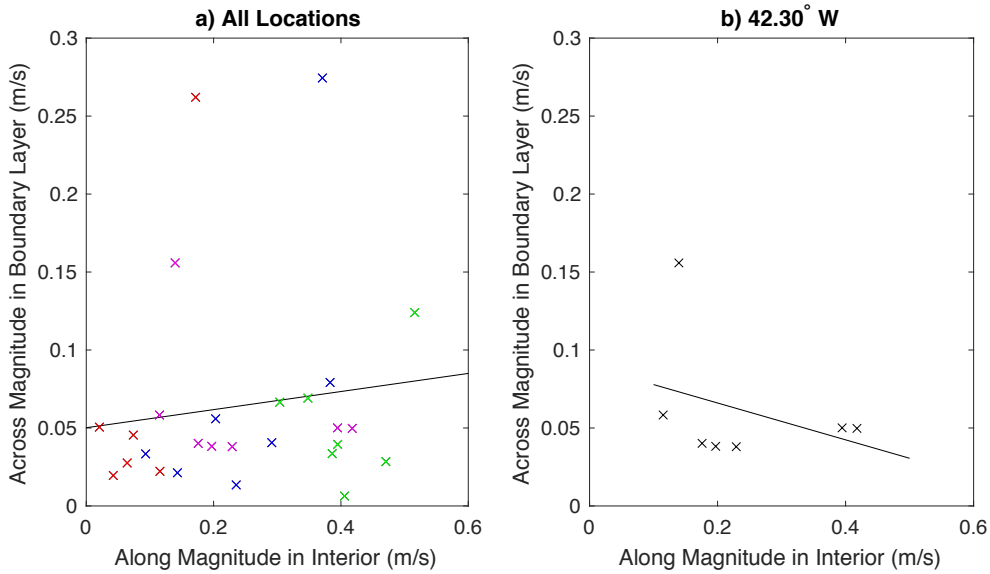

Figure 10: Mean interior along versus mean BBL across magnitudes. a) All transects: 42.15°W (red), 42.20°W (blue), 42.25°W (green) and 42.30°W (magenta) and b) 42.30°W only.

4.4 Does the Across Slope Flow Conform to Ekman Theory?

Nine locations observed as exhibiting across slope flow were found to violate Ekman transport due to the interior across slope velocities being rotated in the opposite direction than dictated by Ekman theory. Ekman theory states that flow within the boundary layer is rotated to the right (clockwise) relative to the overlying interior flow as you approach the seabed. Therefore, if the interior along slope is westward (eastward) you would expect any across slope flow within the boundary layer to be northward (southward). In addition to this, a further three locations were found to violate Ekman theory as the mean magnitude of the along slope BBL velocities exceeded the mean interior along slope velocities. Ekman theory states that the along slope velocities at the seabed are reduced to zero and increase in magnitude with height above the seabed until outside the BBL. In summary, for all four transects, at least one location violates Ekman theory, the transects with the most locations that are found to violate Ekman theory are 42.15°W and 42.30°W, with al l but one location violating Ekman theory at 42.30°W.

Based on the first three steps outline in Section 3.3, this results in six locations that exhibit downslope flow but only somewhat conform to Ekman theory and another two that have a combination of upslope and downslope flow and somewhat conform. There is also one location (42.20°W) where upslope flow is present in the BBL and appears to somewhat conform to Ekman theory.

4.5 Ekman Layer Thickness

Figure 4-Figure 7 show the across slope transects from 42.15°W-42.30°W respectively, positive (negative) across slope flow indicates upslope (downslope) flow. The red lines and blue lines are the BBL thicknesses calculated by methods 1 and 2 respectively. For all locations, method 2 gives thicker Ekman layers than method 1. The thickest Ekman layers were calculated for 42.25°W whilst the thinnest were found at 42.15°W. For each transect, overall the Ekman layer thickness increased downslope.

5 Discussion

5.1 Overview

The majority of locations exhibiting a component of across slope flow in the BBL is consistent with Ekman theory. As summarised by Simpson and Sharples (2010), geostrophic flow (the Taylor-Proudman theorem) breaks down under one of three scenarios: 1) if the flow is unsteady, 2) the flow is so vigorous that the non-linear terms become important, 3) frictional effects are important. As the flow is near the seabed, seabed friction is the most likely cause for the observed ageostrophic flow in the BBL. Furthermore, as the majority of across slope flow is observed in a downslope direction, this is consistent with Polzin *et al.* (2014) who observed a downwelling Ekman layer in the western OP based on data from the ALBATROSS survey (Naveira Garabato *et al.*, 2002) which used LADCPs to asses the flow.

A downwelling Ekman layer would explain a decrease in potential temperature along isobaths. As indicated by the net across slope transport increasing downstream of 42.15°W. Increased downslope flow as you move along the isobaths would result in increased advection of the water with a higher potential downslope that is then transported along isobaths.

According to Ekman theory, due to the influence of seabed friction the along slope flow is brought to rest at the seabed. If Ekman veering is the only process responsible for the behaviour of flow in the BBL you would expect the magnitude of the BBL along slope flow to be less than the magnitude in the interior. This is the reasoning behind the three locations found to violate Ekman theory in Section 4.4. Although along slope flow is brought to rest at the seabed, an increase in the mean interior along slope flow would result in an increase in the mean BBL along slope flow. Therefore, a strong correlation of $R^2 = 0.82$ to a 99% confidence level between the mean along slope flow in the interior and BBL is consistent with Ekman theory.

If the interior flow is entirely geostrophic the across slope flow should be close to 0m/s, Figure 2 and Figure 8 show this is true for the majority of locations between 42.15°W and 42.30°W. Subsequently, it is expected that the magnitude of the mean across slope flow is strongest in the BBL. As indicated in Figure 9, only 11 out of the 28 locations (39%) follow this. And a relatively weak correlation, $R^2 = 0.115$ to a 92% confidence level, is calculated. This indicates that Ekman veering may not be the only process responsible for the observed across slope flow in the BBL. Furthermore, if the interior along slope flow increases, due to seabed friction the across slope flow should increase in the BBL due to the rotation of the current to

the right (clockwise) of the overlying flow as you approach the seabed. A very weak correlation, $R^2 = 0.0158$ to a 47% confidence level for the four transects combined, further indicates that Ekman veering is not the only process responsible for the dynamics within the BBL. When looking at the above correlation for the four transects individually, it its clear that some transects appear to support Ekman veering more than others, for example the strongest correlations are observed at 42.15°W. It is important to note however; correlation doesn't necessarily mean causation. Hence, each location is assessed according to the steps in Section 3.3. The results of the first three steps are shown in Figure 8 which highlights that there is no consistent trend between the locations that conform to Ekman veering and the correlations for each transect.

The rest of this discussion will focus on each of the nine locations identified in Figure 8 that appear to conform to Ekman veering as assessed by the first three steps outlined in Section 3.3. The discussion will also suggest other processes that may be responsible for the observed across slope flow.

5.2 Locations That Somewhat Conform to Ekman Theory

According to Ekman theory as you approach the seabed the current is rotated to the right (clockwise) of the overlying flow direction in the Southern Hemisphere, setting up an Ekman spiral as shown in Figure 11. This spiral can also be visualised by plotting a hodograph of the current vectors as shown in Figure 12. This figure is based in the Northern Hemisphere, therefore in the Orkney Passage, you would expect the hodograph to look like a reflection in the y-axis. The interior flow would be along the x-axis in the westward direction and as you approach the seabed the current vectors are rotated in a clockwise direction away from the interior flow. As Ekman theory is based on a highly idealised scenario and the near seabed velocities are relatively small, a perfect Ekman spiral is very rarely observed in the ocean (Simpson and Sharples, 2010). Therefore, this study will use the net direction of the rotation to further support if Ekman veering is responsible for the across slope flow observed at the nine locations that were found to somewhat conform to Ekman theory based on the first three steps in Section 3.3.

By plotting hodographs, net clockwise rotation was observed at five locations whilst net anticlockwise rotation was observed at four locations as you approach the seabed. For the four locations where net anticlockwise rotation was observed it can be concluded that the locations violate Ekman veering and some other process must be responsible for the across slope flow observed at this location. For three locations (Groups 5 and 6 at 42.25 and group 6 at 42.30°W) where net clockwise rotation was observed, data was only available in the BBL from 40-50m. Based on this data the locations conform to Ekman veering but due to the lack of near seabed

data it cant be concluded that Ekman veering is the only process responsible for the observed dynamics at these locations. The remaining two locations where net clockwise rotation is observed as you approach the seabed will now be discussed further.

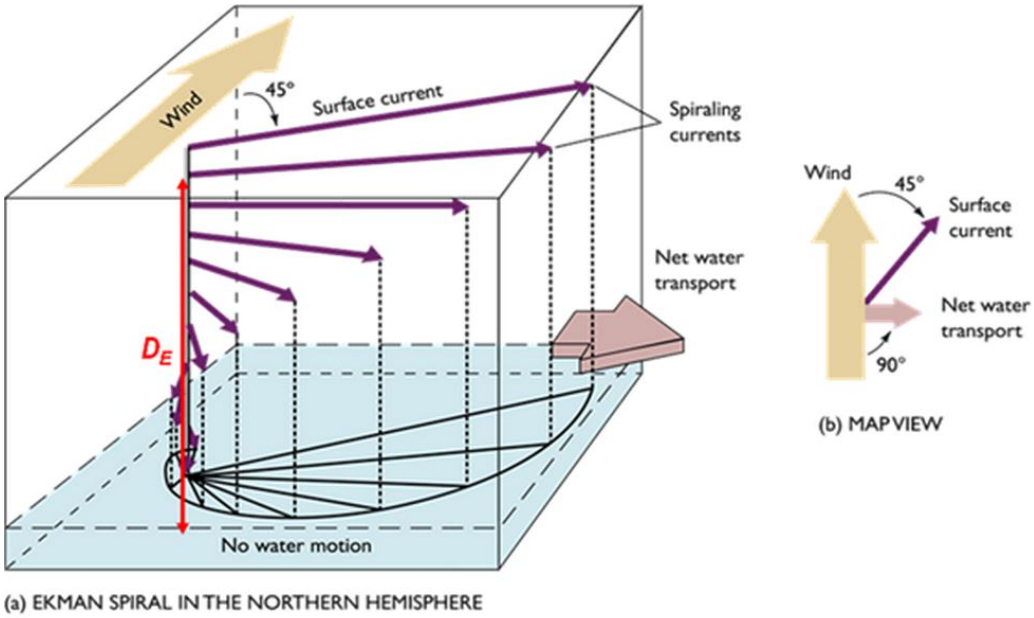

Figure 11: Idealised Ekman Spiral for the sea surface in the Northern Hemisphere (Offshore Engineering, 2016). This is analogous to an Ekman Spiral in the BBL of the ocean in the Southern Hemisphere, where the wind arrow is the interior flow and the surface current is the layer directly beneath the interior in the BBL.

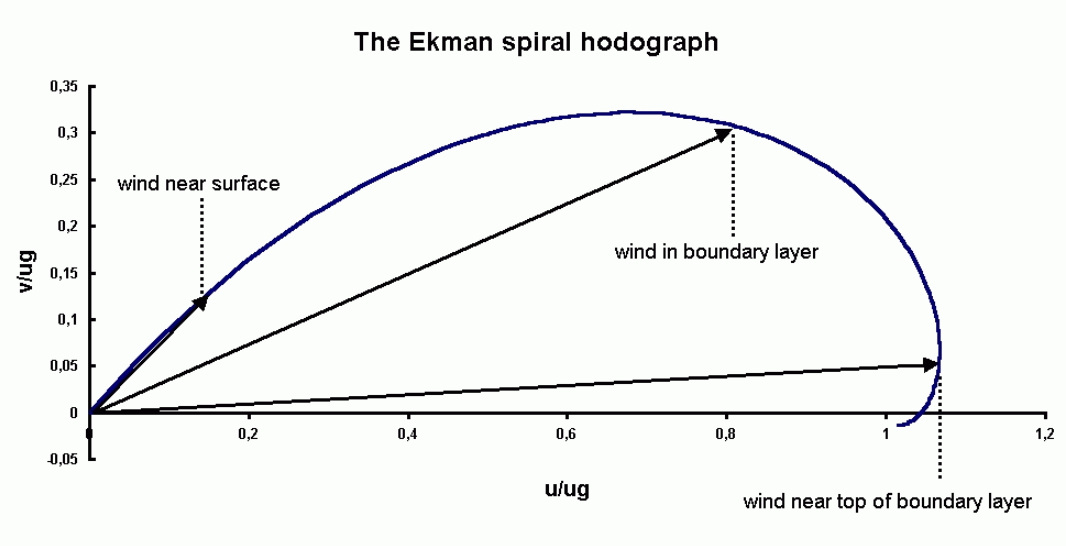

Figure 12: Idealised hodograph for the atmospheric boundary layer in the Northern Hemisphere (EUMeTrain, 2014). For the BBL in the Orkney Passage, the idealised hodograph would appear as a reflection in the y-axis. The wind near the top of the boundary layer is equivalent to the layer furthest away from the seabed in the BBL and the wind near the surface is equivalent to a layer near the seabed.

5.2.1 Group 4, 42.15°W

This is the only location on the 42.15°W transect observed to somewhat conform to Ekman theory. The location is characterised by westward and downslope flow from 8-32m and westward flow (no across slope flow component) from 32-50m as shown in Figure 13. Further analysing the location, a hodograph (Figure 13) was produced from the velocity vectors. This reveals that there is a net clockwise rotation of the current vectors as you approach the seabed. However, the rotation isn't consistently in a clockwise direction throughout the water column. For example, there is anticlockwise rotation from Bins 6-5 and 4-2. As a perfect Ekman spiral is very rarely observed in the ocean (Simpson and Sharples, 2010), the fact that there is net anticlockwise rotation observed in the BBL provides strong evidence that Ekman veering is indeed present in the BBL.

From 8-16m the along slope velocity increased with height above the seabed before decreasing to a constant velocity at 32m above the seabed. At this depth the across slope velocity also remains constant implying the Ekman Depth extends to approximately 32m, this is 20m thicker than calculated by either method in Section 3.4. The mean along slope interior velocity was the same as the mean BBL along slope velocity to two significant figures, under Ekman theory you would expect the interior along slope velocity to be larger than in the BBL (as discussed in Section 5.1). This implies that Ekman veering is only somewhat responsible for the dynamics observed in the BBL at this location.

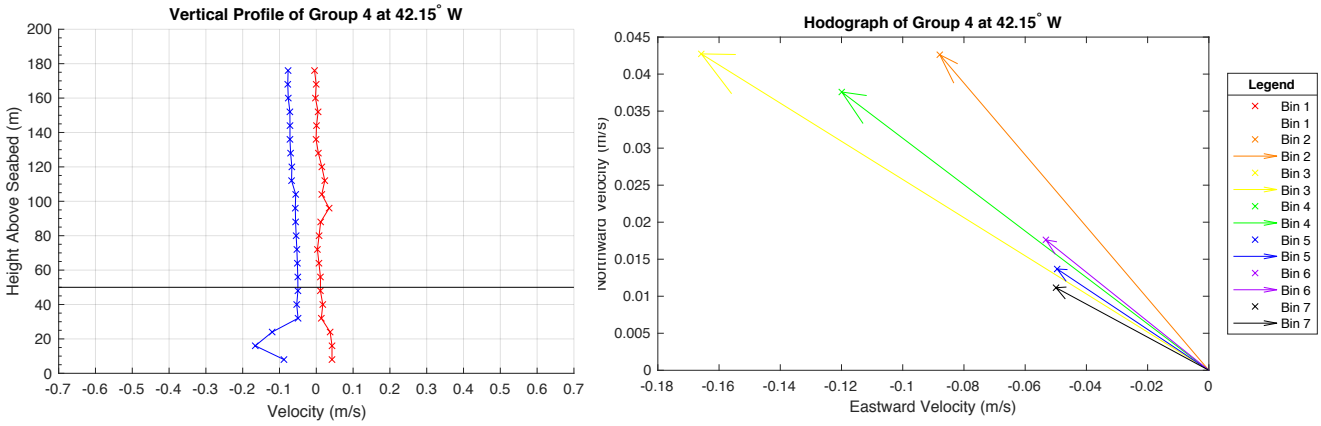

Figure 13: a) Vertical profile of Group 4 and 42.15°W, the blue line is the along slope flow and the red line is the across slope flow. A constant BBL of 50m is denoted by the black line. A positive along and across slope velocities are defined as Eastward and Northward respectively. B) Hodograph of Group 4 at 42.15°W. The bin numbers increase in 8m increments with height above the seabed throughout the depth of the BBL.

5.2.2 Group 5, 42.20°W

At this location the current rotates from eastward and upslope, to westward and downslope, then to westward and along slope. As shown in the hodograph (Figure 14), this is consistent with Ekman veering as the current is rotated clockwise as you approach the seabed. The nearest bin to the seabed (Bin 3) is in an upslope direction, Ekman theory dictates that the spiral rotates to a depth of $z=D_E$ where the current direction is reversed, hence you wouldn't expect an upslope component in the flow. As the perfect Ekman spiral is rarely observed this observation is still reasonable.

However, bins 3 and 4 have relatively large velocities and you would expect this to increase in height above the seabed. But the overlying three bins have relatively smaller velocities. As there is a lack of data near the seabed it can't be determined if bins 3 and 4 are spurious data points or if this trend continues toward the seabed. Large along slope velocities near the seabed would be a violation of Ekman veering, hence it is concluded that these observations alone are not enough to conclude if Ekman veering is the only process responsible for the dynamics in the BBL at this location.

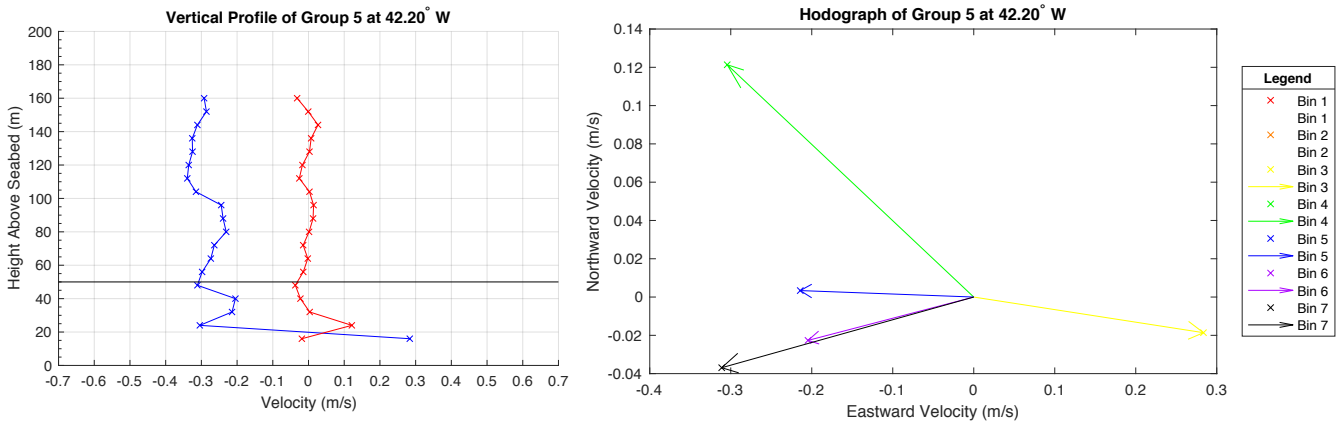

Figure 14: a) Vertical profile of Group 5 at 42.20°W, the blue line is the along slope flow and the red line is the across slope flow. A constant BBL of 50m is denoted by the black line. A positive along and across slope velocities are defined as Eastward and Northward respectively. B) Hodograph of Group 5 at 42.20°W. The bin numbers increase in 8m increments with height above the seabed throughout the depth of the BBL.

5.3 Turbulence

As outline in the introduction and discussed above, regions of high turbulence are associated with Ekman veering (Perlin *et al.*, 2007). Figure 15 shows the dissipation rate from missions M42 and M44 (the basis of this study) from the DynOPO project

(Naveira Garabato *et al.*, 2017). Care must be taken when referring to this figure as Figure 15 uses a different coordinate system to the rest of the figures in this report. Dissipation rates are on a log scale with high dissipation rates indicating regions of high turbulence. By comparing this figure with Figure 2 and Figure 8 it is observed that the dissipation rate increases where the magnitude of the interior flow increases. Due to the influence of seabed friction, flow in the BBL is turbulent (Perlin *et al.*, 2007; Simpson and Sharples, 2010). Therefore, it is expected that locations that exhibit Ekman veering will have increased dissipation rates. Linking Figure 15 to the locations in Sections 5.2.1 and 5.2.2, the dissipation rate was 1×10^{-8} to $1\times10^{-8.5}$ Wkg^{-1} and 1×10^{-9} to 1×10^{-10} Wkg^{-1} for Group 4, 42.15°W and Group 5, 42.20°W respectively. For Group 4 at 42.15°W the dissipation rate is relatively high compared to other locations, supporting that Ekman veering is somewhat responsible for the observed across slope flow. However for Group 5 at 42.20°W the dissipation rate is close to background levels of turbulence, further reinforcing that Ekman veering is not the only process responsible for the across slope flow.

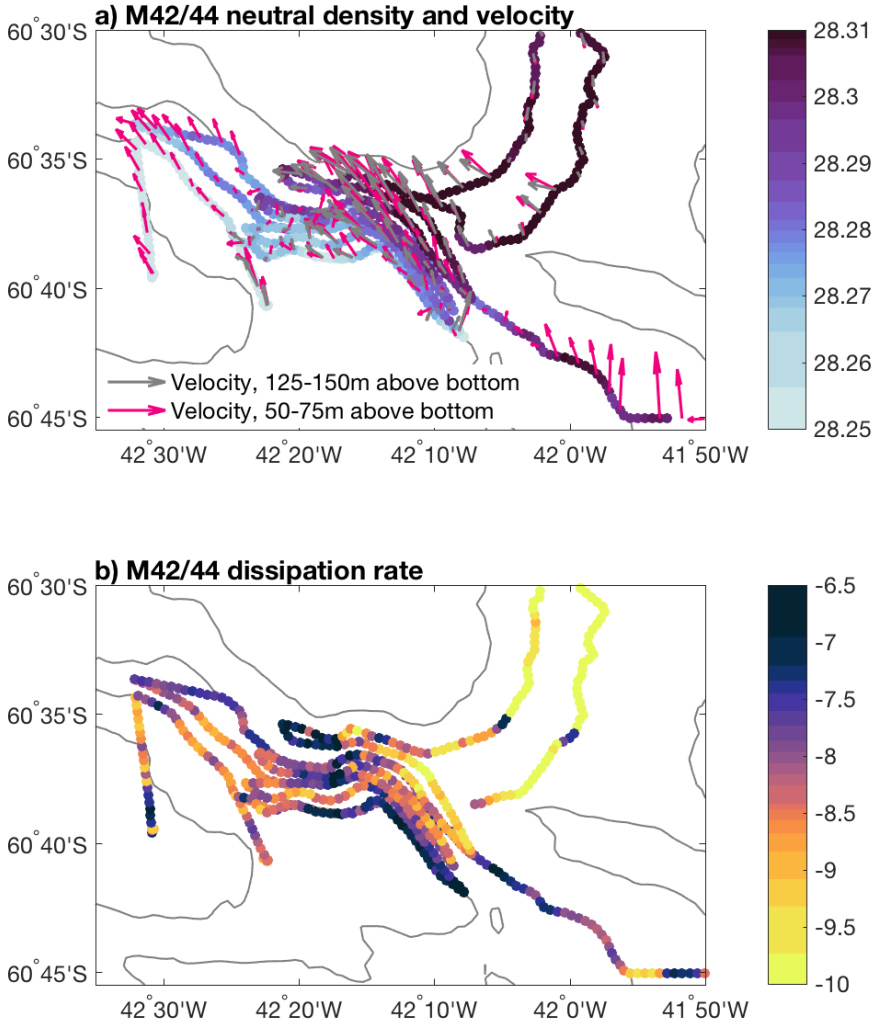

Figure 15: a) Neutral Density (kgm^{-3}). b) Dissipation rate (Wkg^{-1}) from the M42 and M44 ALR mission from the DynOPO project (Frajka-Williams, pers. comm.). Note the different coordinate system used compared to the rest of the figures in this report- this figure has coordinates in degrees, minutes, seconds.

5.4 Other Processes

Downslope flow results in the movement of warm, less dense water from upslope. This sets up a horizontal buoyancy gradient that is associated with strong diapycnal mixing. Polzin *et al.* (2014) observed strong diapycnal mixing in the bottom boundary layer on the western side of the OP and near the sill with values of buoyancy flux in excess of 1×10^{-7} Wkg^{-1}. Some locations had large overturns extending greater than 50-100m in the bottom boundary layer, observed in the vertical profiles where the downslope velocity increases towards the seabed and isopycnals are vertical. This is further supported by Figure 15 which shows dissipation rates in excess of $1\times10^{-6.5}$ Wkg^{-1}. As shown in Figure 16, the vertical density profile from CTD cast 62 is neutrally stratified in the deep ocean and is assumed to extend to the depth of the BBL. Based on the assumption that the near seabed vertical density profiles downstream of this location are similar, this implies isopycnals are titled towards the seabed, consistent with the theory outline in Section 1.2 (Brink and Lentz, 2010). Under these conditions, the across slope buoyancy gradients drive differential across slope advection of less dense water under denser water creating statically unstable conditions and ultimately resulting in overturning. Although mainly in the vertical sense, as turbulence is characterised by the chaotic motion of water particles, this may result in some horizontal flow. Therefore turbulent overturning may be responsible to some extent for across slope flow that is observed at some locations that is rotated in the opposite direction than the overlying interior flow, for example flow that is eastward and downslope in the BBL. Turbulent overturning may also be responsible for the regions with high dissipation rates in Figure 15.

As outlined in Section 1.2 processes other than seabed friction can be responsible for ageostrophic flow. Across slope flow can occur when the flow is unsteady, for example the oscillatory motion of internal tides (Simpson and Sharples, 2010). In addition to the strong diapycnal mixing due to a downwelling Ekman layer observed in the western OP, Polzin *et al.* (2014) hypothesise that the boundary layer dynamics in the western OP are also influenced by the action of semidiurnal internal tides. The topography of the slope on the western side of the OP matches that of semidiurnal internal wave trajectories (Baines, 1974), plus it is known that the southern boundary downstream of the OP is the site of M2 internal tide generation (Padman *et al.,* 2006). Polzin *et al.* (2014) hypothesise this phenomenon is likely to enhance the vertical overturning in the BBL by sustaining vertical sheer and differential advection of density. This is further supported by several pieces of literature that state the near critical reflection of internal waves by a sloping boundary results in enhanced shear and turbulent overturns (Sandstrom, 1966; Eriksen, 1985; Gilbert, 1993; McPhee-Shaw and Kunze, 2002). To conclude,

internal tides may also be responsible to some extent for across slope flow observed in the Orkney Passage.

Another process that is responsible for ageostrophic flow near the seabed is sharp changes in the along slope topography, resulting in the along slope flow to meander or eddy (Simpson and Sharples, 2010). As the along slope current is forced to meander, the non linear terms in the equations of motion become important, hence the flow is no longer geostrophic. This is the most likely process responsible for the strong eastward along slope currents observed at Groups 4 and 5 at 42.30°W. Near 42.25°W there is a bulge in the 2000m isobath. It is hypothesised that this results in eddying behind the feature leading to a reversal of the along slope current. As eddying is associated with turbulent flow, high dissipation rates observed at these locations ($1\times10^{-7.5}$ to 1×10^{-8} Wkg^{-1}) in Figure 15 support this hypothesis. As meandering and eddying results in ageostrophic flow, the process is associated with increased across slope flow (Simpson and Sharples, 2010). At the aforementioned locations, the flow is eastward and downslope throughout the BBL, violating Ekman veering. Further supporting that eddying is most likely responsible for the observed across slope flow. This eddying is also hypothesised to be responsible for the warm patch of water observed along 2750m isobath extending from approximately 42.335-42.355°W as enhanced downslope flow at 42.30°W would result in increased advection of warm water downslope that is then transported along the 2750m isobath.

Meandering flow could further be responsible for the downslope flow observed at Groups 1 and 2 along transect 42.15°W. As observed in Figure 2, there is a very sharp meander in the 1500m, 2000m and 2500m isobath. Any flow encountering these meanders is likely to become ageostrophic and result in across slope flow.

5.5 Ekman Layer Thickness

As shown in Figure 4- Figure 7 the calculated Ekman depth increases downslope, this is consistent with Brink and Lentz (2010). The potential density from CTD cast 62 shown in Figure 16 indicates that the layer immediately above the BBL is likely to be unstratified. This is supported by Polzin *et al.*, (2014) who observed reduced stratification near the boundary region on the western side of the OP. Based on the assumption that the near seabed vertical density profiles downstream of this location are similar, this suggests method 1 is most appropriate to calculate BBL thickness. Price and Sundermeyer (1999) found that as stratification supresses turbulence, under stratified conditions the Ekman layer thins. Hence it should be expected that $\mathrm{D_{E1}}$ is thicker than $\mathrm{D_{E2}}$. However, the opposite is found. Most likely due to $\mathrm{D_{E2}}$ using the buoyancy frequency N calculated under unstratified conditons, resulting in larger than expected values of $\mathrm{D_{E2}}$. This reinforces method 1 being the

most appropriate to calculate the Ekman depth. Furthermore, as indicated in Figure 4-Figure 7, Method 2 appears to overestimate the Ekman depth. For all four transects the maximum D_{E2} exceeded 90m. Plus, at 42.25°W D_{E2} varies from 67-117m this appears to be an overestimation as Ralph and Niiler (1999) state a standard BBL thickness rarely exceeds 60m. This is further supported by Taylor and Sarkar (2008), that state under stratified conditions the Ekman layer is suppressed and has a typical height less than 50m.

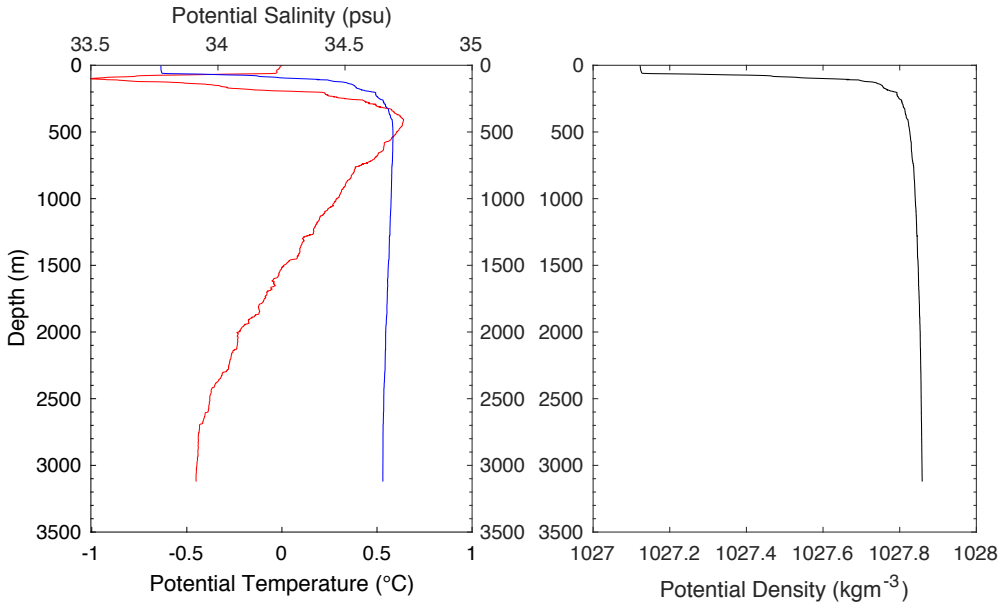

Figure 16: Vertical profile from CTD cast 62. The red line is potential temperature (°C), the blue line is potential salinity (psu) and the black line is potential density (kgm^{-3}).

However, whilst method 1 appears to give a better approximation than method 2, some values calculated by method 1 are very small. For 13 locations the Ekman depth was calculated to be less than 20m. For example at 42.15°W from Groups 1 – 6 the Ekman depth ranges from 0.6-16.5m. The reasoning behind neither method giving a good approximation for the Ekman depth at all locations is because the equations assume that the only processes occurring near the bottom boundary layer is Ekman veering. Due to the extreme small and large values calculated by each method, this suggests that processes other than Ekman veering are occurring within the BBL, consistent with the findings above. It is for this reason that the calculated Ekman depths are not used for an approximation of the BBL thickness. Hence a fixed BBL of 50m is used.

6 Conclusions

This study hypothesises that across slope flow in the western flank of the Orkney Passage will primarily be downslope as a result of Ekman Veering. Across slope flow is observed at 25 out of the 28 locations with downslope flow occurring twice as often as upslope flow. This supports the hypothesis and is consistent with Polzin *et al.* (2014) who observed a downwelling Ekman layer on the western flank of the Orkney Passage.

However, nine locations were found to violate Ekman veering as the across slope flow in the BBL was observed to flow in the wrong direction relative to the overlying interior flow. For example, downslope flow, as observed at some locations, throughout the water column when the interior flow was westward. A further three locations were found to violate Ekman theory as the BBL along slope magnitudes were larger than the interior along slope magnitudes. Both of the above indicate that Ekman veering is not the only process responsible for the observed across slope flow.

Further analysis of the net rotation of the current vectors within the bottom boundary layer reveal a further four locations violated Ekman theory as the net rotation was in an anticlockwise direction as you approach the seabed. Ekman theory stipulates that rotation is in a clockwise direction as you approach the seabed in the Southern Hemisphere. Therefore, it can be concluded that only five locations somewhat conform to Ekman veering being responsible for the observed across slope flow in the BBL. As Ekman theory is based on a highly idealised scenario and Ekman spirals like that in Figure 11 are rarely observed in the ocean (Simpson and Sharples, 2010), the fact that five locations are observed to somewhat conform to Ekman veering is meaningful.

Although it is concluded that Ekman veering is not the only process responsible for the across slope flow observed at the 25 locations, a downwelling Ekman layer would explain a decrease in potential temperature along isobaths. As indicated by the net across slope transport increasing downstream of 42.15°W. Increased downslope flow as you move along the isobaths would result in increased advection of the water with a higher potential downslope that is then transported along isobaths.

Other processes that may be responsible for some of the across slope flow observed at the 25 locations are: vertical overturning due to the across slope horizontal density gradients; the oscillatory motion of internal tides; and meandering/eddying. It is known that the southern boundary downstream of the OP is the site of M2 internal tide generation (Padman *et al.*, 2006) and that the slopes of

the Orkney Passage match semidiurnal internal wave trajectories (Baines, 1974). Polzin *et al.* (2014) hypothesise that the action of internal tides is responsible for enhanced diapycnal mixing in the BBL. Meandering and eddying result in ageostrophic flow when the nonlinear terms in the dynamical equations become important. It is hypothesised that eddying is responsible for downslope flow observed at Groups 4 and 5 at 42.30°W due to a bulge in the 2000m isobath near 42.25°W. This eddying is further hypothesised to be responsible for the warm patch of water observed along the 2750m isobath extending from approximately 42.335-42.355°W.

In terms of calculating the Ekman layer thickness it is concluded that neither method is appropriate. Method 2 was found to give larger thicknesses than method 1 which contradicts the theory that stratification suppresses turbulence in the BBL (Perlin *et al.,* 2007). Whilst Method 1 was found to give very small Ekman layer thicknesses, for example 13 locations had an Ekman layer less than 20m thick. As the equations are based on Ekman veering being the only process responsible for the dynamics in the BBL, this further supports that Ekman veering is not the only process that is responsible for the observed dynamics in the BBL.

In summary, despite the ALR M44 mission providing high resolution near seabed data, it only provides a snapshot of the behaviour of the near seabed flow in the western flank of the Orkney Passage. Whilst it can be concluded that Ekman veering may be somewhat responsible for the observed across slope flow in the region, based on the data from the M44 mission alone it is not sufficient to determine the extent to which other processes that may contribute. Therefore, the findings of this study only somewhat support the hypothesis that across slope flow in the region will primarily be downslope as a result of Ekman Veering.

References

Baines, P. G. (1974). The generation of internal tides over steep continental slopes. Philosophical Transactions of the Royal Society London A. 277, 27–58.

Brink, K. H. and Lentz, S. J. (2010). Buoyancy Arrest and Bottom Ekman Transport. Part I: Steady Flow. Journal of Physical Oceanography. 40, 621-635.

Ekman, V.W. (1905). On the influence of the earth's rotation on ocean-current. Arkiv för Matematik, Astronomi och Fysik. 2(11), 1-53.

Eriksen, C. C. (1985). Implications of ocean bottom reflection for internal wave spectra and mixing. Journal of Physical Oceanography. 15, 1145 – 1156.

EUMeTrain. (2014). Coastal Convergence: Meteorological Physical Background. [Online]. Available from: http://www.eumetrain.org/satmanu/CMs/CoConv/navmenu.php?page=2.0.0. [Accessed 18 March 2018].

Gilbert, D. (1993). A search for evidence of critical internal wave reflection on the continental rise and slope off Nova Scotia. Atmosphere-Ocean. 31, 99 – 122.

Gill, A. E. (1982). Atmosphere-Ocean Dynamics. Academic Press, New York. pp.662. (First Edition).

Gordon, A. L., Visbeck, M. and Huber, B. (2001). Export of Weddell Sea deep and bottom water. Journal of Geophysical Research. 106, 9005–9017.

Hanna, S.R. (1969). The Thickness of the Planetary Boundary Layer. Atmospheric Environment Pergamon Press. 3, 519-536.

Jullion, L., Naveira Garabato, A.C., Bacon, S., Meredith, M.P., Brown, P.J., Torres-Valdés, S., Speer, K.G., Holland, P.R., Dong, J., Bakker, D., Hoppema, M., Loose, B., Venables, H.J., Jenkins, W.J., Messias, M.J. and Fahrbach, E. (2014). The contribution of the Weddell Gyre to the lower limb of the global overturning circulation. Journal of Geophysical Research: Oceans, 119, 3357–3387.

MacCready, P., and Rhines, P.B. (1993). Slippery bottom boundary layers on a slope. Journal of Physical Oceanography. 23, 5–22.

McPhee-Shaw, E. E., and Kunze, E. (2002). Boundary layer intrusions from a sloping bottom: A mechanism for generating intermediate nepheloid layers. Journal of Geophysical Research. 107(C6), 1-16.

Meredith, M. P., Locarnini, R.A., Van Scoy, K.A., Watson, A.J., Heywood, K.J. and King, B.A. (2000). On the sources of Weddell Gyre Antarctic Bottom Water, Journal of Geophysical Research. 105, 1093–1104.

Meredith, M.P., Gordon, Arnold L., Naveira Garabato, Alberto C., Abrahamsen, E. P., Huber, Bruce A., Jullion, Loïc, Venables and Hugh J. (2011). Synchronous intensification and warming of Antarctic Bottom Water outflow from the Weddell Gyre. Geophysical Research Letters. 38 (3), L03603, 1-4.

Naveira Garabato, A. C., Heywood, K.J. and Stevens, D.P. (2002). Modification and pathways of Southern Ocean Deep Waters in the Scotia Sea, Deep Sea Research, Part I. 49, 681–705.

Naveira Garabato, A., Buckingham, C., McAfee, C., Dotto, T.S., Spingys, C.P., Hooley, J., Benson, J., Mountifield, D., Platt, B., Evans, J., Abrahamsen, P., Polzin, K.L., Forryan, A., Brown, N., Davies, A., Frajka-Williams, E. and Nicholls, K. (2017). RRS James Cook Cruise JR16005, 17 Mar - 08 May 2017. The Dynamics of the Orkney Passage Outflow (DynOPO). Southampton, GB. National Oceanography Centre. pp.222. (National Oceanography Centre Cruise Report, 47).

Offshore Engineering. (2016). Ekman Current, Upwelling, Downwelling. [Online]. Available from: http://www.offshoreengineering.com/education/oceanography/ekman-current-upwelling-downwelling. [Accessed 18 March 2018].

Padman, L., Howard, S., and Muench, R. (2006). Internal tide generation along the South Scotia Ridge. Deep Sea Research, Part II. 53, 157–171.

Perlin, A., Moum, J.N., Klymak, J.M., Levine, M.D., Boyd, T. and Kosro, P.M. (2007). Organization of stratification, turbulence, and veering in bottom Ekman layers. Journal of Geophysical Research. 112, C05S90, 1-12.

Pollard, R. T., Rhines, P.B. and Thompson, R. (1973). The deepening of the wind-mixed layer. Geophysical Fluid Dynamics, 4(4), 381–404.

Polzin, K.L., Naveira Garabato, A.C., Abrahamsen, E.P., Jullion, L. and Meredith, M.P. (2014). Boundary mixing in Orkney Passage outflow. Journal of Geophysical Research: Oceans. 119 (12), 8627-8645.

Price, J. F. and Sundermeyer, M.A. (1999). Stratified Ekman layers. Journal of Geophysical Research. 104(C9), 20,467– 20,494.

Purkey, S. G., and Johnson, G.C. (2010). Warming of global abyssal and deep Southern Ocean waters between the 1990s and 2000s: Contributions to global heat and sea level rise budgets. Journal of Climate. 23, 6336–6351.

Ralph, E. A. and Niiler, P. P. (1999). Wind-Driven Currents in the Tropical Pacific. Journal of Physical Oceanography. 29, 2121-2129.

Sandstrom, H. (1966). The importance of topography in generation and propagation of internal waves. Ph. D. Thesis. University of California. pp.105.

Simpson, J.H and Sharples, J. (2010). Introduction to the physical and biological oceanography of shelf seas. Cambridge University Press. pp. 424. (First Edition).

Taylor, R.J. and Sarkar, S. (2008). Stratification Effects in a Bottom Boundary Layer. Journal of Physical Oceanography. 38, 2535-2555.

Trowbridge, J. H. and Lentz, S.J. (1991). Asymmetric behavior of an oceanic boundary layer above a sloping bottom. Journal of Physical Oceanography. 21, 1171–1185.